SIMULATION AND SYMMETRY OF SIMPLE AND COMPLEX FLOWS

M. W. Evans and D. M. Heyes

Department of Chemistry
Royal Holloway and Bedford New College
University of London, Egham, Surrey TW20 OEX, UK

1. INTRODUCTION

In this study we interpret the microscopic simulation of flows in a new way, making use of the flow and property symmetry as embodied in the *new* principles of group theory statistical mechanics.

The hydrodynamics of complex flows is a subject which has been based historically on constitutive equations derived from the fundamental equations of motion in the classical approximation.[1,2] This approach "washes out" the microscopic structure of the fluid, and is forced to ignore the fact that this is generally molecular in nature. D.J. Evans has shown that the constitutive equations for a molecular (structured) fluid such as carbon tetrachloride become numerous, complicated, and insoluble within the reasonable future.[3] The many body dynamics are traditionally kept under control by approximations which not only ignore the existence of molecules but which also lead to severe contemporary controversy over frame indifference, a problem arising *purely* from the constitutive equation methodology.[4]

The consequencies of ignoring the details of molecular dynamics in fluids under elongational and shear stress include the following.

1) The constitutive approach remains empirical, *i.e.*, 'Newtonian' or 'non-Newtonian' according to whether the stress / strain relation appears linear or not.

2) Empiricism, as usual, means that the traditional approach is not predictive, but descriptive, in nature. A general solution of flow in atomic or molecular ensembles requires the fundamental equations of motion in the classical approximation applied to the many body problem through computer simulation.

3) The constitutive approach misses some fundamental details of the response of fluids to shear stress.[5–7] This happens even in the 'simplest' of fluids, composed of atoms. Examples of this basic weakness in the constitutive approach are given later in this article.

4) The computer power needed to implement the constitutive approach is about the same as that needed in the more fundamental approach made possible by

Microscopic Simulations of Complex Flows
Edited by M. Mareschal, Plenum Press, New York, 1990

recent advances in computer simulation. So we might as well use the latter whenever possible.

5) The fundamental approach attacks problems at the fundamental level, and once these are solved, a new world of possibilities is there for the exploration. It becomes possible, for example, to implement group theory and symmetry to reveal the presence of indicator functions which appear in a fluid in response to shear. Their presence leads directly to new types of spectra which are characteristic of the rheology of a sheared liquid. An example is depolarised light scattering.[8]

Recent work, using nonequilibrium molecular dynamics (NEMD) and Brownian dynamics (BD) simulation has shown that the response of an atomic ensemble to shear and elongational stress is a rich landscape of interwoven patterns, a picture which can be drawn in terms of cross correlation functions (c.c.f.'s) governed by the three principles of group theoretical statistical mechanics (g.t.s.m.).[9-15] Time correlation functions in the transient (non-equilibrium) state can be used to generalise the Green-Kubo relations and linear response theory in one simple and elegant equation.[16] The third principle of g.t.s.m. applies also to these transient c.c.f.'s, and is ideal for the description of shearing and elongational stress in terms of symmetry. In molecular liquids considerations of symmetry apply not only in the laboratory frame (X, Y, Z) but also in the molecule fixed frame (x, y, z) as defined in the standard point group character tables.[17,18] This implies that the response of a molecular fluid under complicated external stress can be analysed precisely with a variety of new indicator c.c.f.'s in both frames. Not only are these symmetry-specific to the type of stress (shear, elongation, compression, or any combination, [19-21]) but also to the point group of the molecule in frame (x, y, z). The effect of stress can be studied in both frames (X, Y, Z) and (x, y, z) by NEMD and Brownian Dynamics, BD simulation,[22,23] implementing the SLLOD equations, profile unbiased thermostatting (PUT) or any other numerical technique.

This represents a significant advance over the constitutive approach to rheology, which is not able to describe flow at the atomic or molecular level, and in consequence is not able to describe or anticipate the existence of indicator c.c.f.'s.

Another major advantage of the fundamental approach is that it reveals phenomena on the picosecond/angstrom scale of a computer simulation which remain valid on the second/metre scale of laboratory and industrial flow processes. This follows quite clearly from the fact that the classical equations of motion are valid on both scales. A one-to-one relation can be developed straightforwardly between simulation and observation, and it follows that the former is capable of predicting experimental observables on the second/metre scale. Several master curve and extrapolative techniques for doing just this have been developed recently by Heyes and co-workers.[23,24] It follows that in the design of specific materials with specific and predictable response to imposed stresses of various kinds, fundamental computer simulation is the obvious answer.

The fundamental technique has been applied with notable success by Rapaport and co-workers,[25] and by Clementi and co-workers[26-29] to flows around objects on the picosecond/angstrom scale, revealing on this scale the presence of vortices, eddies, and other flow phenomena whose behaviour extrapolates linearly to the second/metre scale. These phenomena obey symmetry principles that can be used to relate them to indicator c.c.f.'s at the fundamental level and thus to close the gap between traditional

hydrodynamics and molecular dynamics. Some of these symmetries are discussed later, in the context of flow past objects, hydrodynamic instability (Rayleigh-Benard phenomena), and in other less well-known contexts such as rotating electric fields as first tackled by Born,[30] in the early twenties of this century and demonstrated experimentally by Lertes,[31], Grossetti,[32], and Dahler,[33]. This elegant work shows that spinning electric fields can physically rotate a liquid at up to MHz frequencies, and is the historical precursor of electrorheology, an important contemporary technique. G.t.s.m. can be applied in all these contexts, and in combination with NEMD and BD simulation, has already produced indications of the presence of explanations and phenomena unknown to the constitutive approach. Examples described later include 1) the first explanation for the Weissenberg effect in terms of pressure tensor correlation functions; 2) the discovery by combined simulation/symmetry of thermal conductivity produced by simultaneous shear and elongational stress in atomic ensembles.

2. SYMMETRY AND FLOWS

Symmetry is simple and powerful, and its application to complicated flow is no exception. Of key importance in this application are the three principles of g.t.s.m.,[11-15] recently developed and stated in terms of contemporary point group theory. The first principle is the Neumann/Curie Principle applied with group theory, and states that the ensemble average over a product of scalars, vectors or tensors exists in the laboratory frame if its product of representations contains at least once the totally symmetric irreducible representation of $R_h(3)$, the point group of all rotations and reflections. If the ensemble is chiral, the relevant point group becomes $R(3)$ of all rotations. The second principle applies principle (1) to the molecule fixed frame (x, y, z), where the relevant totally symmetric irreducible representation is that of the molecular point group, e.g. C_{2v} for water or T_d for carbon tetrachloride etc. The third principle is a simple but very powerful cause effect theorem which states that if an external field of force is applied to an ensemble of atoms or molecules, that ensemble develops transient or steady state ensemble averages with the same symmetry as that of the applied field itself. In other words the symmetry of cause and effect is identical.

Principle (3) is found to be particularly useful for NEMD and BD simulation of complicated flows. It applies across the whole of mechanics, classical, statistical, quantum and grand unified, and also in other contexts, such as classical, quantum, and relativistic electromagnetic field theory, both in linear and non-linear contexts.

In order to implement these principles it is necessary to define the irreducible representations of scalar, pseudoscalar, vector and tensor quantities in the point group of interest. In the context of principle three, the field symmetry is defined through these irreducible representations in the point group of the ensemble (i.e. $R_h(3)$ or $R(3)$). For $R_h(3)$ the set of irreducible representations consists of the the D representations, $D_g^{(0)}, \ldots\ldots D_g^{(n)}$ and $D_u^{(0)}, \ldots\ldots, D_u^{(n)}$. In $R(3)$ the set consists of, $D^{(0)}, \ldots\ldots, D^{(n)}$. Thus, scalar, vector, or tensor quantities in $R_h(3)$ can be either positive (g) or negative (u) to the parity inversion operation, which takes (X, Y, Z) to (-X, -Y, -Z) and which is defined as the operation, $\hat{P} : (r, p) \rightarrow (-r, -p)$, where r and p denote position and linear momentum respectively. Of additional interest is the time reversal operator, defined as $\hat{T} : (r, p) \rightarrow (r, -p)$. In $R(3)$ the g and u subscripts are undefined because the $\hat{P}$ operator takes the ensemble to the opposite enantiomer, a distinctly different entity, and is therefore not a valid group theoretical operation.

In $R_h(3)$ a scalar quantity such as mass is $D_g^{(0)}$; a pseudoscalar is $D_u^{(0)}$; a polar vector such as linear momentum or position is $D_u^{(1)}$; an axial vector such as angular velocity or vortex is $D_g^{(1)}$; and higher order tensors are u or g. The totally symmetric irreducible representation is $D_g^{(0)}$. In $R(3)$ the same definitions apply without subscripts, so that the symmetries of a scalar and pseudoscalar are identical in $R(3)$; as are those of polar and axial vectors and so on. The totally symmetric irreducible representation is $D^{(0)}$. In order to build up the symmetries of ensemble averages over products of two or more quantities, such as time c.c.f's of the generic type $< A(0)B(t) >$, we use the Clebsch Gordan Theorem,

$$D^{(n)}D^{(m)} = D^{(n+m)} + D^{(n+m-1)} + \ldots\ldots\ldots + D^{(|(n-m)|)}, \tag{1}$$

with the rule for subscript multiplication, $gg = uu = g; ug = gu = u$, in $R_h(3)$. If we are dealing with the nine element tensor $< v(t)v(0) >$, where v is atomic or molecular centre of mass velocity, for example, the product of representations in $R_h(3)$ is,

$$\begin{aligned} R_h(3) : \Gamma(v)\Gamma(v) &= D_u^{(1)}D_u^{(1)} \\ &= D_g^{(0)} + D_g^{(1)} + D_g^{(2)}, \end{aligned} \tag{2}$$

so that the signature of the complete c.c.f. tensor is the sum of scalar, vector and second rank tensor symmetries. The complete tensor is overall positive to $\hat{P}$ and $\hat{T}$. Similarly, the signature of the c.c.f. $< v(t)\omega(0) >$, where v and ω are respectively the linear and angular velocities of a diffusing molecule, is

$$\begin{aligned} R_h(3) : \Gamma(v)\Gamma(\omega) &= D_u^{(1)}D_g^{(1)} \\ &= D_u^{(0)} + D_u^{(1)} + D_u^{(2)}, \end{aligned} \tag{3}$$

which is negative to $\hat{P}$ and positive to $\hat{T}$.

In the point group $R(3)$ of chiral ensembles the representation of both c.c.f.'s is the same,

$$R(3) : \Gamma(v)\Gamma(v) = \Gamma(v)\Gamma(\omega) = D^{(0)} + D^{(1)} + D^{(2)}, \tag{4}$$

with positive time reversal symmetry. Principle (1) shows therefore that the scalar component of $< v(t)v(0) >$ exists in $R_h(3)$ but all elements of $< v(t)\omega(0) >$ vanish. In $R(3)$ the $D^{(0)}$ element of the latter c.c.f. exists as a pseudoscalar quantity. To apply principle (3) we need to examine the symmetries of flow fields in both point groups. Some examples of cause and effect relations obeying principle (3), together with their $\hat{P}$, $\hat{T}$ and D symmetries are as follows,

Linear force: Acceleration, - , +, $D_u^{(1)}$

Torque: Angular acceleration, + , + , $D_g^{(1)}$

Electric field (E): Polarisation, -, +, $D_u^{(1)}$

Electric field (E): $< v(t)\omega(0) >$, -, +, $D_u^{(1)}$

Magnetic Field (B): Magnetization, + , -, $D_g^{(1)}$

Shear Stress: Off diagonal $< v(t)v(0) >$, + , +, $D_g^{(1)} + D_g^{(2)}$

Elongational stress: Diagonal $< v(t)v(0) >$, +, + ,$D_g^{(0)}$

Rotating E: Bulk rotation, +, -, $D_g^{(1)}$

Above, the first entry records Newton's second law of motion, whereby force results in a net acceleration of an N body ensemble with the given symmetries. An intrinsically time independent electric field of force results in dielectric polarisation, which is an ensemble average of the same symmetry over permanent electric dipole moments. Less obviously, the electric field also causes the vector part of the c.c.f. matrix $< v(t)\omega(0) >$ to appear in frame (X, Y, Z), a result first noted in the mid-eighties using conventional computer simulation in molecular liquids.

Stress is the negative of the pressure tensor, which is force divided by a scalar unit volume cross section. Stress therefore has the symmetry of its equivalent force field, and principle three may be used to find the symmetry of the ensemble averages set up by stress. These are the same symmetries as strain rate multiplied by a scalar viscosity, in general the nine element tensor product of velocity and inverse position,

$$\Gamma(v)\Gamma(1/r) = D_g^{(0)} + D_g^{(1)} + D_g^{(2)}, \tag{5}$$

with negative $\hat{T}$. Shear stress and strain rate symmetry is the off-diagonal part, made up of a combination of symmetry $D_g^{(1)}$ (vorticity) and $D_g^{(2)}$ (deformation). Elongational stress and strain rate symmetry is the diagonal part, $D_g^{(0)}$. Combined shear and elongational stress (complex stress) produces a response with the complete D symmetry on the right hand side of eqn. (5).

In the context of complex stress we arrive at the important conclusion that ensemble averages of the same symmetry are set up by principle (3) in frame (X, Y, Z) of the laboratory. Among these are a new and useful class of indicator c.c.f.'s exemplified by $< P_{XY}(0)P_{YZ}(t) >$ for the pressure tensor components and $< v(t)v(0) >$, whose characteristics have been described recently by Evans and Heyes using $SLLOD$, PUT, and BD simulation.[34,35]

3. INDICATOR C.C.F'S, THE SIGNATURES OF COMPLEX FLOW

These are available only from the fundamental $NEMD$ and $NEBD$ computer simulation methods developed in the past few years, and appear to be inaccessible to the traditional constitutive description of stress induced flow. The work of Evans and Heyes has shown that the indicator c.c.f. $< v(t)v(0) >$ for shear stress has the unique property of being neither symmetric nor antisymmetric to index reversal (or the equivalent time displacement),[9]

$$< v_X(t)v_Z(0) > \neq < v_Z(t)v_X(0) >, \tag{6}$$

in the steady state under applied shear. (Here the shear rate is $\dot{\gamma} = \partial v_X/\partial Z$.) This property appears to be the first counter-example to the Onsager/Casimir Reciprocal Principle, which demands symmetry or antisymmetry, but cannot account for asymmetry, in X and Z. The same time asymmetry arise in the c.c.f.'s of the pressure tensor (zero in the absence of shear). Illustrations of this new and unique property are provided from $SLLOD$ and PUT simulations in figs. 1 and 2 in the two and three dimensional fluid states.

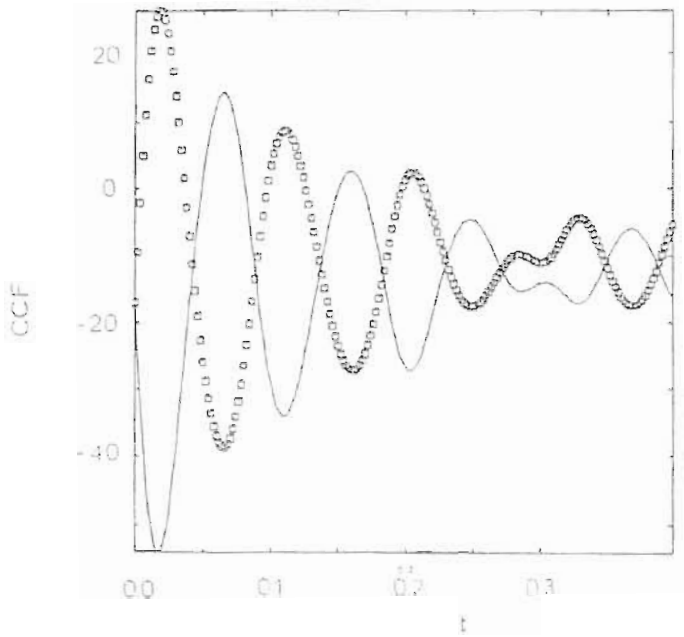

Fig. 1 The time cross-correlation function $(V/k_BT) < P_{XY}(0)P_{YZ}(t) >$, solid line and $(V/k_BT) < P_{YZ}(0)P_{XY}(t)$, squares using the PUT algorithm ($r_p = 2\sigma$) at the $3D$ LJ $N = 500$ state $\rho = 0.8442$, $T = 0.722$ and $\dot{\gamma} = 20$.

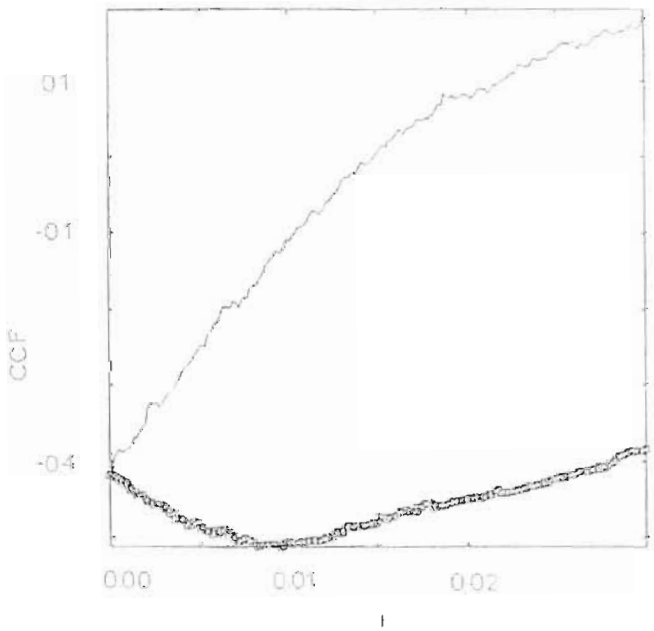

Fig. 2 The time correlation function, $< v_X(0)v_Z(t) >$, squares, and $< v_Z(0)v_X(t) >$, solid line for $2D$ soft-disk states at $\rho = 0.733, T = 1.0$ and $\dot{\gamma} = 17.8$ using the PUT algorithm.

The indicator c.c.f. in eqn (6) has the overall D, $\hat{P}$ and $\hat{T}$ symmetries of the above list from principle three, *i.e.*, a *weighted* combination of $D_g^{(1)}$ and $D_g^{(2)}$. This is a weighted combination of,

$$D_g^{(1)} :< v_X(t)v_Z(0) >= - < v_Z(t)v_X(0) >, \tag{7}$$

and

$$D_g^{(2)} :< v_X(t)v_Z(0) >=< v_Z(t)v_X(0) >, \tag{8}$$

i.e., of antisymmetric shear induced vortex flow and symmetric shear induced deformational flow. The combined effect (eqn. (7)) is neither symmetric nor antisymmetric, and is therefore called "asymmetric" (non-Onsager/Casimir) flow. The complete D symmetry of the macroscopic stress field downstream of the disk is therefore,

$$D_g^{(0)} + D_g^{(1)} + D_g^{(2)}, \tag{9}$$

implying the existence of all elements of the indicator c.c.f. tensor $< v(t)v(0) >$. The explorative work and conclusions of Evans and Heyes on combined shear and elongational flow,[19] may therefore be applied to the region downstream of the disk in two dimensions, or cylinder in three. For example, we expect the presence downstream of asymmetric, non-Onsager/Casimir, c.c.f.'s of velocity, position, mixed velocity and position, and various asymmetric c.c.f.'s of pressure tensor components coming from the shearing part of the complete downstream stress field symmetry. We expect symmetric diagonal components of these fundamental indicator correlation functions due to the elongational part of the complete downstream stress field. These functions would be the microscopic signature of the macroscopic flow phenomena discussed by Clementi and co-workers,[25–28] *i.e.*, eddies, vortices, and so on, the conventional hydrodynamic description. On a more fundamental level, these are described by indicator cross correlation functions.

As shown by Evans and Heyes, the shear and elongational parts of the complete stress field are mutually interdependent. The time evolution of the respective indicator c.c.f.'s would likewise depend on each other, but *not* the symmetry, which is an ineluctable signature of the elongational, or alternatively of the shearing, component of the complicated macroscopic flow. Interestingly, the flow combined downstream stress field symmetry is expected to produce thermal conductivity, defined as the Green-Kubo (or the more general Morriss-Evans) integral over the heat flux tensor of Irving and Kirkwood. The D symmetry of the downstrean stress field remains the same for more complicated objects, such as an ellipse, or an object shaped like a car body, aircraft wing, or ship's hull. Downstream turbulent behaviour, lift, and so on are characterised therefore by these indicator c.c.f.'s on a fundamental level, and this should be of direct use in industrial design processes, based on the flow of air or water past macroscopic objects in NEMD or NEBD simulations.

4. SYMMETRY OF MACROSCOPIC FLOW CREATED BY A ROTATING DISK

A rotating macroscopic disk in an N body ensemble creates a macroscopic flow consisting of vorticity and elongational shear, the symmetry of whose strain rate tensor is, $D_g^{(1)}(-) + D_g^{(2)}(-)$ in $R_h(3)$. The time reversal symmetry in brackets is negative. The equivalent stress field tensor has the same D symmetry, but is positive to $\hat{T}$, generated by the fact that stress is a $\hat{T}$ negative strain rate tensor multiplied by

a scalar $\hat{T}$ negative viscosity. By principle (3), the stress field causes an effect of the same symmetry, which may be measured through the same asymmetric indicator c.c.f.'s, positive to $\hat{T}$, as described by Evans and Heyes in the context of couette flow.[9]

The flow created by a rotating disk therefore has the same non-Onsager Casimir characteristics as those of couette flow. These fundamental, microscopic, indicator c.c.f.'s are functions of the visible, macroscopic, non-Newtonian rheology of the fluid. In some cases, stirring (rotating macroscopic rod) causes the fluid to solidify (cornflour paste), a response which is a non-Newtonian in the extreme. In this case the asymmetric indicator c.c.f. in the shear-induced solid state would be highly oscillatory and very asymmetric. In the context of stirred liquid crystals, the same non-Newtonian characteristics dominate, some liquid crystals having the property of acting like clockwork springs, once wound up (stirred) they unwind again at a different pace after the stirrer is switched off. In this case the fundamental, indicator c.c.f.'s are going to be highly asymmetric.

In fig. (3) we show the velocity flow lines around two counter-rotating solid disks in a $2D$ LJ fluid. Note the symmetry breaking aspects of the flow lines. In fig. (4) we show the associated density variation in the configuration. The major density variations at different points in the flow field reveal the power of the microscopic simulation technique in accounting for the many-body properties *in situ*.

5. FLOW FROM ROTATING ELECTRIC AND ELECTROMAGNETIC FIELDS

Mechanical shear rates cannot exceed about a megahertz. This limits experimental investigation to these frequencies. In contrast, the strain rates of a typical NEMD or NEBD simulation are in the megahertx (MHz) to terahertz (THz) range. It would be of interest to stir a fluid in the mechanically inaccessible MHz to GHz range to complete the investigation of its non-Newtonian response. This is easily possible in principle with contemporary technology by using the Born/Lertes effect.[30,31] Among Max Born's earliest contributions was a theoretical paper published in 1920,[30], which showed that a liquid suspended between rotating electric fields in a thin walled glass vessel on a torsion wire produces a measurable torque. Born analysed the effect in terms of the Debye relaxation time, showing that the effect maximises at the Debye peak frequency corresponding to the Debye relaxation time. This was confirmed almost immediately by Lertes.[31] Further exparimental work was reported more than thirty years later by Grossetti,[32] and a masterly teatment by Dahler appeared in 1965.[33] The Born/Lertes effect seems not to have been utilised to investigate the non-Newtonian rheology of fluids, but allows such work to proceed with rapidly spinning electric fields or circularly polarised lasers, in which the electric field spins about the propagation axis. The complete D symmetry of the macroscopic stress field downstream of the disk is therefore, $D_g^{(0)}+D_g^{(1)}+D_g^{(2)}$, implying the existence of all elements of the indicator c.c.f. tensor $< v(t)v(0) >$. The original Born/Lertes effect has the D, $\hat{P}$ and $\hat{T}$ symmetries of a rotating electric field. The electromagnetic equivalent, which seems not to have been described in the literature, involves the same symmetry, that of the rotating electric field component of the circularly polarised electromagnetic field. The nearest equivalent to the electromagnetic Born/Lertes effect is the discovery by Beth,[36] that a circularly polarised laser rotates an optically birefringent crystal suspended on a torsion wire. This was used as one experimental proof of the fact that a photon has spin, i.e. is a chiral particle travelling at the speed of light.

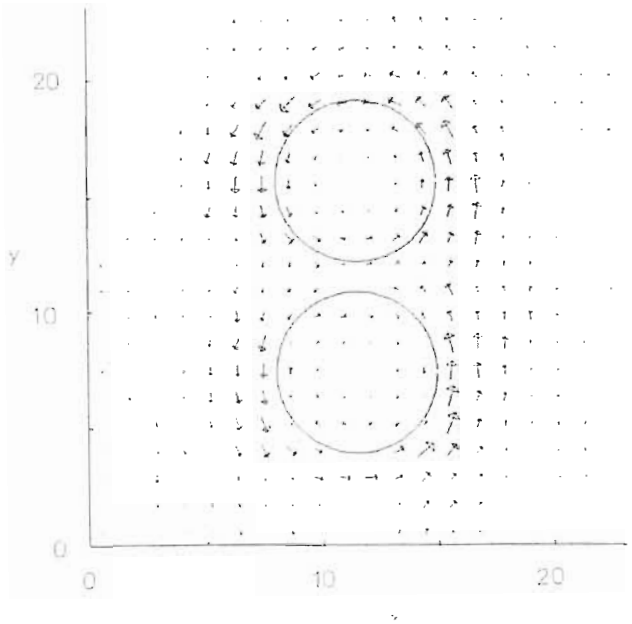

Fig. 3 Grid velocities around two counter-rotating $2D$ disks in a $2D$ Lennard-Jone fluid. The average density is $\rho = 0.75$ and $T = 0.6$. $N = 400$, $\delta t = 0.015$, thermostatted by velocity rescaling. The sidelength is $S = 23.1\ LJ\sigma$. The radius of each solid LJ disk is $0.15 \times S$. The length and direction of each arrow indicates the relative magnitude and direction of the the flow velocity in the grid domain. The maximum velocity shown os 0.33 LJ reduced units. Note the symmetry breaking of the flow lines around the two disks.

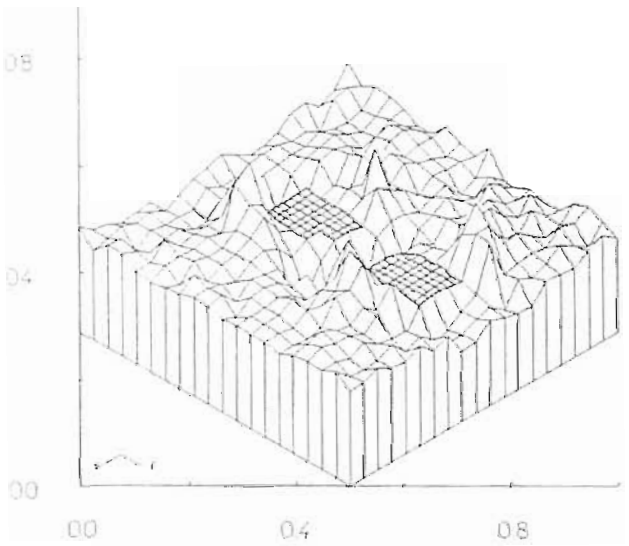

Fig. 4 The fluid density contours for the state of Fig. 3. For clarity the two disks are assigned zero density, therefore appearing as voids in the middle of the figure (as finer grids). The peak density in the figure is 1.41 reduced units. Notice the enhanced fluid density around the fluid disk peripheries.

The tip of the rotating electric field vector draws out a circle, and the overall symmetry is the same as that of a shear stress field, *i.e.*, $D_g^{(1)}(+) + D_g^{(2)}(+)$, where $D_g^{(1)}$ refers to $\nabla \times E$, the curl, which through Maxwell's equations is minus the time derivative of the magnetic field, and the $D_g^{(2)}$ refers to the off-diagonal part of the dyadic ∇E. Dahler,[33] has clearly analysed the macroscopic flow set up by the electric field with analytical hydrodynamics. The above rotating electric field symmetry is imparted by principle three to the molecular ensemble contained in the suspended thin walled sphere, provided that the molecules have a permanent electric dipole moment. We expect off diagonal, asymmetric, indicator c.c.f.'s of the type $< A(t)A(0) >$ where A is molecular centre of mass velocity, dipole moment, angular velocity, and so on to appear in a computer simulation analysis of this effect. The electric field gradient has the same symmetry as a stress tensor, and sets up a shear in the ensemble.

The D symmetry of the rotating electric field includes that of angular acceleration, or torque, $D_g^{(1)}(+)$, which causes the entire vessel to accelerate rotationally against the torsion wire in the Born/Lertes experiment, following the simple cause/effect principle three. This torque is a direct measure of non-Newtonian effects and is dependent on an effective viscosity in the same way as mechanical stress is viscosity multiplied by mechanical strain rate. The strain rate due to the rotating electric field has, $D_g^{(1)}(-)+D_g^{(2)}(-)$, symmetry, which includes the $D_g^{(1)}(-)$ symmetry of macroscopic angular momentum, angular velocity, vortex, or magnetic field. The advantage of using the Born/Lertes effect to study non-Newtonian macroscopic flow is that the rotating electric field frequency can be varied over the Hz to upper MHz range using four electrodes arranged around the sample suspended in the thin walled vessel from the torsion wire. The macroscopic torque depends on the Debye relaxation time as shown by Born, and confirmed by Dahler's extensive analysis. The Debye relaxation time is dependent on the viscosity as is well known in dielectric relaxation. From the MHz range upwards into the far infra red (to about 100 THz) the rotating electric field can be generated by circularly polarised electromagnetic radiation, and here again we expect the appearance of asymmetric indicator c.c.f.'s as the beam becomes elliptically polarised due to sample absorption through the molecular permanent dipole moment.[37] Here again, the maximum torque on the torsion wire appears at the inverse of the Debye relaxation time, which under certain circumstances occurs in the microwave frequency range just below the far infra red. This brings the experimental study within the range of computer simulation of shear stress phenomena. We mention in concluding this section that the non-Newtonian nature of the response of the sample can also be measured through the time dependent magnetization set up by the curl of the electric field.

6. THE SYMMETRY AND COMPUTER SIMULATION OF CHANNEL FLOW

The characteristics of macroscopic channel flow have recently been studied by Lie and co-workers using computer simulation and stochastic hydrodynamics.[38,39] Using two dimensional computer simulations with thermal walls, these authors have described the velocity and temperature characteristics of very dilute gases in channel flow, and have begun to investigate the effects of density variation across a temperature gradient in a three dimensional system. They have also simulated Rayleigh Benard phenomena and hydrodynamic instabilites and cell patterns using upwards of a quarter of a million particles and specialised boundary conditions. This work shows clearly the advantages of the fundamental approach, and shows a number of features

which are again inaccessible to the constitutive approach.

The D, $\hat{P}$ and $\hat{T}$ symmetry of the stress field in channel flow is, $D_g^{(0)}(+) + D_g^{(1)}(+) + D_g^{(2)}(+)$, and the indicator function, $< v(t)v(0) >$, contains all nine elements in general by principle three. The elongational stress field dominates near the channel centre away from the walls and the shear stress field dominates near the walls. Lie and co-workers describe the resulting velocity profile for various Knudsen numbers, which on average shows a well defined parabolic character. This much is known hydrodynamically, but the fundamental approach goes deeper, and may examine the root cause of this in terms of indicator c.c.f. symmetries at the flow applied steady state. It is significant that Lie et al. measure a heat dissipation by viscous dissipation as the density of the ensemble decreases, one symptom of which is increased velocity near the thermal walls of the flow channel. This appears to support the conclusions of Evans and Heyes in another context, described already, where combined elongational and shear flow results in heat flux and thermal conductivity. There is also a temperature profile across the flow channel which is a kinetic energy profile related to the square of the velocity. In channel flow we may therefore expect indicator c.c.f.'s of non-Onsager/Casimir symmetry, and also diagonal elements of the indicator c.c.f.'s. The off-diagonal elements dominate near the walls and the diagonal elements near the channel centre, thus explaining the observed velocity profile on a fundamental level.

7. HYDRODYNAMIC INSTABILITY AND RAYLEIGH-BENARD PATTERNS

The symmetries of hydrodynamic instability arise from convection when, for example, a fluid is heated from below. These Rayleigh-Benard patterns have recently appeared from a fundamental computer simulation.[40] Hydrodynamical instability and the Rayleigh-Benard problem are usually treated with an infinite layer of fluid in which a steady adverse temperature gradient is maintained, usually by heating from below. This implies a pressure and density distribution as well as a thermal gradient. Rayleigh analysed the early observations of Benard of cell structures due to this hydrodynamic instability by building up triangular, quadrilateral, and hexagonal cells using classical hydrodynamic theory. He showed that the component of horizontal velocity perpendicular to the cell walls observed by Benard disappears.

A recurring D symmetry in the Rayleigh Benard problem is, $D_u^{(1)} D_u^{(1)} D_u^{(1)}$, *i.e.*, the cube of $D_u^{(1)}$.This occurs in such quantities as the gradient of the pressure tensor (positive $\hat{T}$), the pressure distribution caused by hydrodynamic instability (heating a liquid from below). It also occurs with negative $\hat{T}$ symmetry in the equations governing velocity within the Rayleigh Benard cells, a typical scalar component of which is, $(n.\nabla)v = 0$, where n is a unit vector perpendicular to the cell wall. The presence of a temperature gradient implies a heat flux tensor J, which in the Irving/Kirkwood definition has the same D symmetry as the gradient of the pressure tensor but is negative to $\hat{T}$.

The cell patterns emerge from Rayleigh's analysis by considering equations which contain scalar components of the second gradient of velocity and the gradient of the vorticity, which both have the same general $D, \hat{P}$ and (negative) $\hat{T}$ symmetries as the Irving/Kirkwood heat flux tensor J. The thermal conductivity is the Green-Kubo, or more generally, the Morriss-Evans, integral over the correlation function of J. With these symmetries we note that principle (3) applies to the Rayleigh-Benard problem and its complicated macroscopic cellular flow patterns as follows. The cause (external

field) in principle (3) is a heat flux, which has the units of force gradient per unit volume cross section (the same units as the gradient of the pressure tensor); and one of the effects is represented by the scalar element $(n.\nabla)v$ which vanishes at the cell walls. This is the same $\hat{P}, \hat{T}$ and D symmetry, and governs the Rayleigh-Benard cell patterns. Principle (3) relates the symmetry of the heat flux tensor directly to the symmetry of the Rayleigh-Benard macroscopic flow cells. We have reduced the complicated Rayleigh-Benard macroscopic flow problem to a $(D_u^{(1)})^3$ symmetry. This can be rewritten as the product, $D_u^{(1)}(D_g^{(0)}+D_g^{(1)}+D_g^{(2)})$, one of whose two components is the combined symmetry of the indicator c.c.f. $< v(t)v(0) >$. In the Rayleigh-Benard cells, therefore, we expect non-Onsager Casimir off-diagonal elements of $< v(t)v(0) >$ and symmetric diagonal elements, the former predominating near the cell walls and the latter near the centre of the macroscopic flow cells. Interestingly, the Rayleigh-Benard D symmetry also allows all scalar elements in general of the triple indicator correlation function $< vvv >$. The latter is unique to Rayleigh-Benard flow and computer simulation should reveal many of its interesting features.

8. CONCLUDING REMARKS

Several different macroscopic flow problems recently treated by microscopic computer simulation have been analysed and reduced to combinations of D symmetries of the point group $R_h(3)$. The elongational stress field has symmetry $D_g^{(0)}(+)$; the shearing stress field is a linear combination of the vorticity component of $D_g^{(1)}(+)$ symmetry, and the deformational component of $D_g^{(2)}(+)$ symmetry. The combined elongation and shear stress field is a linear combination of these three D components. In channel flow, $D_g^{(0)}(+)$ dominates near the channel centre, and $D_g^{(1)}(+) + D_g^{(2)}(+)$ near the walls. In the Born/Lertes effect, the rotating electric field sets up $D_g^{(1)}(+) + D_g^{(2)}(+)$ macroscopic flow; and Rayleigh Benard hydrodynamic instability has the symmetry signature $(D_u^{(1)})^3$. Principle three of g.t.s.m. applies to all these complicated macroscopic flows, and shows the presence of indicator c.c.f.'s of each type of flow. Some components of the indicator c.c.f.'s break Onsager/Casimir symmetry (vortex and deformational shear flow), others are symmetric diagonal (elongational flow). The Rayleigh Benard cells allow both types, together with scalar components of the triple indicator c.c.f $< vvv >$.

Acknowledgements

D.M.H. gratefully thanks *The Royal Society* for the award of a *Royal Society 1983 University Research Fellowship.* M.W.E. thanks RHBNC for the award of an Hon. Research Fellowship. We thank S.E.R.C. for the award of computer time at the University of London Computer Centre, and the RHBNC Computer Center for use of their VAX 11/780 computer facilities.

References

1. J. Harris, "Rheology of non-Newtonian Flow", Longman, London (1977).

2. B. C. Eu, J. Chem. Phys., 82:3773 (1985).

3. D. J. Evans, Mol. Phys. 42:1355 (1981).

4. A. S. Lodge, R. B. Bird, C. F. Curtiss, and M. W. Johnsson, J. Chem. Phys., 85:2341 (1986).

5. M. W. Evans and D. M. Heyes, Mol. Phys., 65:1441 (1988).

6. M. W. Evans and D.M. Heyes, Physica Scripta, in press (1988).

7. M.W. Evans and D.M. Heyes, J. Mol. Liq., in press (1988).

8. M. W. Evans, Mol. Phys., in press (1988).

9. M.W. Evans and D.M. Heyes, Mol. Phys. 65:1441 (1988).

10. D. M. Heyes, Computer Phys. Rep., 8:71 (1988).

11. M. W. Evans, Chem. Phys. Lett., 152:33 (1988).

12. M. W. Evans, Phys. Lett. A, 134:409 (1989).

13. M. W. Evans, Chem. Phys., 127:413 (1988); 132:1 (1989).

14. M. W. Evans, Physica B, 154:313 (1989).

15. M. W. Evans, Phys. Rev. A, 39:6041 (1989).

16. G. P. Morriss and D. J. Evans, Phys. Rev. A, 35:792 (1987).

17. R. L. Flurry, Jr., "Symmetry Groups, Theory and Chemical Applications.", Prentice Hall, Englewood Cliffs (1980).

18. F. A. Cotton, "Chemical Applications of Group Theory", Wiley Interscience, New York (1963).

19. M. W. Evans and D. M. Heyes, Mol. Phys., submitted for publication.

20. L. D. Landau and E. M. Lifshitz, "Fluid Mechanics", Pergamon, Oxford (1959).

21. A. Garcia, Phys. Rev. A, 34:1454 (1986).

22. D. M. Heyes, J. Chem. Soc., Faraday Trans. 2, 82:1365 (1986).

23. D. M. Heyes and R. Szczepanski, J. Chem. Soc., Faraday Trans. 2, 83:319 (1987).

24. D.M. Heyes and J.R. Melrose, Mol. Sim. 2:281 (1989).

25. D. Rapaport and E. Clementi, Phys. Rev. Lett., 57 (1986)

26. L. Hannon, G. C. Lie and E. Clementi, J. Stat. Phys., 51:965 (1988).

27. ibid., Phys. Lett. A, 119:174 (1986).

28. A. L. Garcia, M. M. Mansour, G. C. Lie, and E. Clementi, Phys. Rev. A, 36:4348 (1987).

29. M. W. Evans, G. C. Lie, and E. Clementi, Phys. Rev. A, 37:2551 (1988).

30. M. Born, Z. Phys., 1:221 (1920).

31. P. Lertes, ibid., 4:315 (1921); 6:56 (1921); 22:261 (1921).

32. E. Grossetti, Il Nuovo Cimento, 10:193 (1958); 13:621 (1959).

33. J. S. Dahler, in "Research Frontiers in Fluid Dynamics", (ed. R. J. Seeger and G. Temple, Interscience, New York, (1965).

34. M. W. Evans and D.M. Heyes, J.C.S. Faraday Trans 2, submitted.

35. M.W. Evans and D.M. Heyes, Mol. Sim. submitted.

36. R.A. Beth, Phys. Rev., 50:115 (1936).

37. M.W. Evans, Chem. Phys. Lett., (1989) in press.

38. M.M. Mansour. A.L. Garcia, G.C. Lie and E. Clementi, Phys. Rev. Lett., 58:874 (1987).

39. D.K. Bhattacharya and G.C. Lie, Phys. Rev. Lett, 62:897 (1989).

40. J.A. Given and E. Clementi, J. Chem. Phys., 90:7376 (1989).